npj | climate and atmospheric science

Article

Published in partnership with CECCR at King Abdulaziz University

https://doi.org/10.1038/s41612-025-00899-z

Future large-scale atmospheric circulation changes and Greenland precipitation

Baojuan Huai[1], Minghu Ding[2] ✉, Michiel R. van den Broeke[3], Carleen H. Reijmer[3], Brice Noël[4], Weijun Sun[1] & Yetang Wang[1]

In this work, we examine connections between patterns of future Greenland precipitation and large-scale atmospheric circulation changes over the Northern Hemisphere. In the last three decades of the 21st century, CMIP5 and CMIP6 ensemble mean precipitation significantly decreases over the northern part of the North Atlantic Ocean with respect to 1951–1980. This drying signal extends from the ocean to the southeastern margin of Greenland. The 500 hPa geopotential height change shows a clear pattern including a widespread increase across the Arctic with a negative anomaly centered over Iceland and surrounding regions. To identify the mechanisms linking atmospheric circulation variability with Greenland precipitation, we perform a singular value decomposition (SVD) and center of action (COA) analysis. We find that a northeastward shift of the Icelandic Low (IL) under the SSP5-8.5 warming scenario leads to the drying signal found in southeast Greenland. This implies that the IL location will have a strong influence on precipitation changes over southeast Greenland in the future, impacting projections of Greenland ice sheet surface mass balance.

The Arctic climate is changing rapidly, far beyond what is expected from natural variability[1,2]. As a consequence, the Greenland ice sheet (GrIS) has been losing mass since the 1990s[3–5], and the decreasing surface mass balance (SMB) dominates the mass loss over the GrIS since 2000[6]. If Greenland warming reaches 4.5 ± 0.3 °C by the year 2055, the SMB is projected to become negative initiating sustained surface mass loss[7]. By the end of the 21st century, the ensemble mean projections of GrIS surface mass loss contribute to a mean sea level rise (SLR) of 4 ± 2 cm and 9 ± 4 cm for the RCP (Representative Concentration Pathways) 4.5 and RCP8.5 scenarios, respectively[8,9].

Precipitation (snowfall plus rainfall) is the main positive contributor to the mass balance of the GrIS[10,11]. Therefore, accurate quantification of contemporary and projected precipitation changes is crucial to estimate GrIS mass change[12]. The contemporary Greenland precipitation pattern is shaped by storm track activities and transient large-scale weather systems associated with lifting effect of topography of the ice sheet. Its spatial distribution is characterized by onshore flow/precipitation maxima along the south and southeast flank of Greenland and offshore flow/drier conditions in the northeast and central Greenland[13,14]. From thermodynamic considerations, it has been hypothesized that climate warming should be accompanied by a precipitation increase over Greenland[15], following the Clausius–Clapeyron relationship which states that saturated atmospheric moisture content increases by ~7% per degree of warming[16]. Such an increase could partly compensate for melt-induced mass loss. Yet, regional climate models and airborne radar observations indicate that contemporary GrIS precipitation has remained relatively constant[17–19], with a possible small increase over parts of the interior[20,21].

Throughout the remainder of the 21st century, sustained atmospheric warming, followed by increased surface melt and runoff, is expected to cause continued GrIS mass loss[22], but the potential future mitigating role of increasing precipitation remains elusive[23,24]. The marked increase in precipitation in the Arctic region (70°–90°N), which is among the strongest globally, is attributed primarily to enhanced poleward moisture transport[25]. Other studies used global climate models to show that projected Arctic precipitation increases by more than 50% at the end of the 21st century[16,26,27].

The amount of precipitation is regulated primarily by atmospheric conditions, such as stability, water-vapor content[28], and atmospheric circulation[29–31], in combination with surface topography. A northward shift in the mid-latitude storm track results in less precipitation over the southeast coast of Greenland[32,33], with an increase in precipitation over the

[1]College of Geography and Environment, Shandong Normal University, Jinan, China. [2]State Key Laboratory of Severe Weather, Chinese Academy of Meteorological Sciences, Beijing, China. [3]Institute for Marine and Atmospheric Research, Utrecht University, Utrecht, The Netherlands. [4]Laboratory of Climatology and Topoclimatology, Department of Geography, University of Liège, Liège, Belgium. ✉e-mail: dingminghu@foxmail.com

southwest coast and east Greenland. There have been a handful of other studies relating Greenland precipitation to the large-scale atmospheric circulation[34–36], showing that the North Atlantic Oscillation (NAO) most strongly modulates precipitation in west and south Greenland. Other studies explored the influence of the Atlantic Multi-decadal Oscillation (AMO), Icelandic Low (IL), Azores High (AH), regional blocking patterns, and near-surface temperature and winds. These studies showed that correlations are significant and stronger between Greenland precipitation and the IL than either the NAO or AMO indexes[29]. In years when the IL is positioned anomalously far to the west, moisture transport increases to southeast Greenland[34]. Previous studies argue that a better understanding of climatic events in the North Atlantic can be obtained by analyzing the pressure centers of the IL and AH as uncoupled rather than combined as in the NAO index[37]. NAO evolution in a global warming projection from the ECHAM4/OPYC3 coupled general circulation model, which showed that the annual meridional pressure gradient over the North Atlantic is significantly strengthened, and IL and AH, the two centers of action (COA), are both intensified and shifted northeastward by 10° to 20° in latitude and 30° to 40° in longitude in the period 2000–2099[38].

The coupled model intercomparison project (CMIP)[39] offers the opportunity to further explore Greenland historical and future precipitation under different warming scenarios[40–42] and the mechanisms driving these changes[4]. In this study, to further examine patterns of future precipitation change over Greenland, we use a large ensemble of the Coupled Model Inter-comparison Project Phase 5 and 6 (CMIP5 and CMIP6, respectively). We investigate a possible dynamic linkage between Greenland precipitation changes and circulation anomalies over the Northern Hemisphere by using Singular Value Decomposition (SVD) and COA location shift analysis. As CMIP6 models capture the relationships between the atmospheric circulation anomalies and precipitation changes, we then calculate the COA indexes to examine these changes, which provide useful insights into projected climate changes over Greenland and the surface mass balance of the GrIS.

Results

Projected Greenland precipitation changes and atmospheric circulation anomalies

To evaluate CMIP6 model performance, we compared historical precipitation (1951–2014) with ERA5. Figure S1 in Supplementary Material shows the differences in annual precipitation between each CMIP6 model, the multi-model ensemble mean (MME), and ERA5, indicating that the CMIP6 models have a large inter-model spread. This can be attributed to both differences in natural variability and model uncertainties. Model differences (CMIP6 minus ERA5) are mostly lower than 2 SD relative to the ERA5 precipitation (1951–2014) for four CMIP6 models, including UKESM1-0-LL, HadGEM3-GC31-LL, EC-earth3 and CESM2-WACCM, meaning that their simulated precipitation fields are consistent with the ERA5 climate reanalysis.

To illustrate the individual model precipitation trends in detail, Fig.1 shows precipitation trends (2015–2100) in all CMIP6 models under the SSP5-8.5 scenario. All CMIP6 models show a positive trend in northern Greenland, which is therefore also present in the CMIP6 multi-model mean (Fig. 2), although the magnitude of the precipitation trend can differ among CMIP6 models. But for southeast Greenland where precipitation peaks, the trends vary widely among CMIP6 models, which suggest that precipitation trends in southeast Greenland remain elusive. In some of the models (i.e., CESM2, CESM2-WACCM, EC-earth3, GISS-E2 and etc.) a significant negative precipitation trend is found in southeast Greenland and the surrounding regions, while for other models a positive trend is found. The precipitation increase in northeast Greenland is potentially associated with sea ice loss in the 21st century[16], as the expansion of open water leads to enhanced atmospheric instability, surface evaporation, atmospheric condensation, moisture content, and precipitation. The study also suggested that, due to a northward shift in the storm tracks, synoptic patterns that favor precipitation over northern and eastern Greenland become more frequent during the 21st century[24].

Despite these model uncertainties, the multi-model ensemble means of the CMIP5 and CMIP6 are used to analyze 21st century changes in Greenland precipitation characteristics. Figure 2 compares the last three decades of the 21st century (2071–2100, P2) to the baseline period (1951–1980, P1) for both ensemble means of the CMIP5 and CMIP6 models. From the low to high-emission scenarios, the spatial patterns of precipitation change remain consistent, with the largest increase in south Greenland and the smallest increase in the high interior.

Compared to the historical period P1, period P2 shows a decrease in precipitation over the North Atlantic Ocean, which in all three scenarios is better defined in the CMIP6 ensemble (Fig. 2). This decrease in precipitation over the ocean does not reach the GrIS interior in either CMIP5 or CMIP6 models. Some models (i.e., CMCC-ESM2, CanESM5, INM-CM4-8, IPSL-CM6A-LR and etc.) show significant positive trends in southeast Greenland and the surrounding regions (Fig. 1) relative to the models mentioned above. Therefore, a decreasing precipitation signal in the southeastern GrIS in the multi-model ensemble mean is likely overwhelmed by the larger increase in some GCMs. However, the CMIP6 ensemble mean does show a precipitation decrease extending from the ocean to the southeastern Greenland margin.

Figure S2A shows time series of the Greenland precipitation first empirical orthogonal function (EOF1) pattern from 39 CMIP6 models under the SSP5-8.5 scenario during 1951–2100. The ensemble mean time series of the normalized annual precipitation index in the northwest (red) and southeast (blue) Greenland are also shown. Interestingly, EOF1 patterns from 20 out of 39 CMIP6 models show a precipitation dipole pattern between northwest and southeast Greenland. These dipole patterns result in opposite ensemble mean precipitation trends over southeast and northwest Greenland ($R = -0.42$), indicative of opposite northwest and southeast Greenland precipitation variations. The dipole pattern found in EOF1 explains 20–64% of the precipitation variance among the 39 models. From the multi-model ensemble, mean normalized Greenland precipitation anomaly during 1951–2100 (Fig. S2B), both the southeast and northwest Greenland precipitation changes manifest a year-to-year variation during 1951–2100. More than half (20 out of 39) of the selected CMIP6 models capture this dipole oscillation pattern well, which can also be seen from standardized interannual precipitation anomalies (Fig. S2B). These results support that the dipole pattern in Greenland precipitation could likely form in the future, with a leading role for large-scale atmospheric circulation mechanisms, which will be further examined below.

These future precipitation changes (Figs. 1, 2, and S2) can be related to atmospheric circulation changes over Greenland[43]. Figure 3 shows the annual 500 hPa geopotential height (Z500) and change between period P2 and P1 for both the CMIP5 (Fig. 3a) and CMIP6 (Fig. 3b) ensemble mean under the SSP5-8.5 scenario. The circulation change patterns are similar for the CMIP5 and CMIP6 ensemble means, and in the Greenland region are characterized by two regions of positive anomalies to the west and east, flanking a negative anomaly centered over Iceland and surrounding regions (Fig. 3). The largest positive Z500 anomalies are projected over the Eurasian region with mean increases of 22 gpm in CMIP5 and 24 gpm in CMIP6, respectively. This anomaly weakens the west-to-east circulation (zonal flow) and enhances meridional fluxes. This intensifies heat and moisture transport from the south to the GrIS, and dampens subsidence in the northern part of Greenland, resulting in higher precipitation over northeast Greenland (Fig. 2). These results agree with the study using three selected AOGCMs from IPCC AR4[13]. The negative Z500 anomaly centered over Iceland exceeds −25 gpm in both the CMIP5 and CMIP6 ensemble mean.

Connections between Greenland precipitation changes and atmospheric circulation anomalies

To explore linkages between the atmospheric circulation anomalies and Greenland precipitation changes, we perform singular value decomposition (SVD), spatial distribution of covariance analysis, for Z500 in the non-

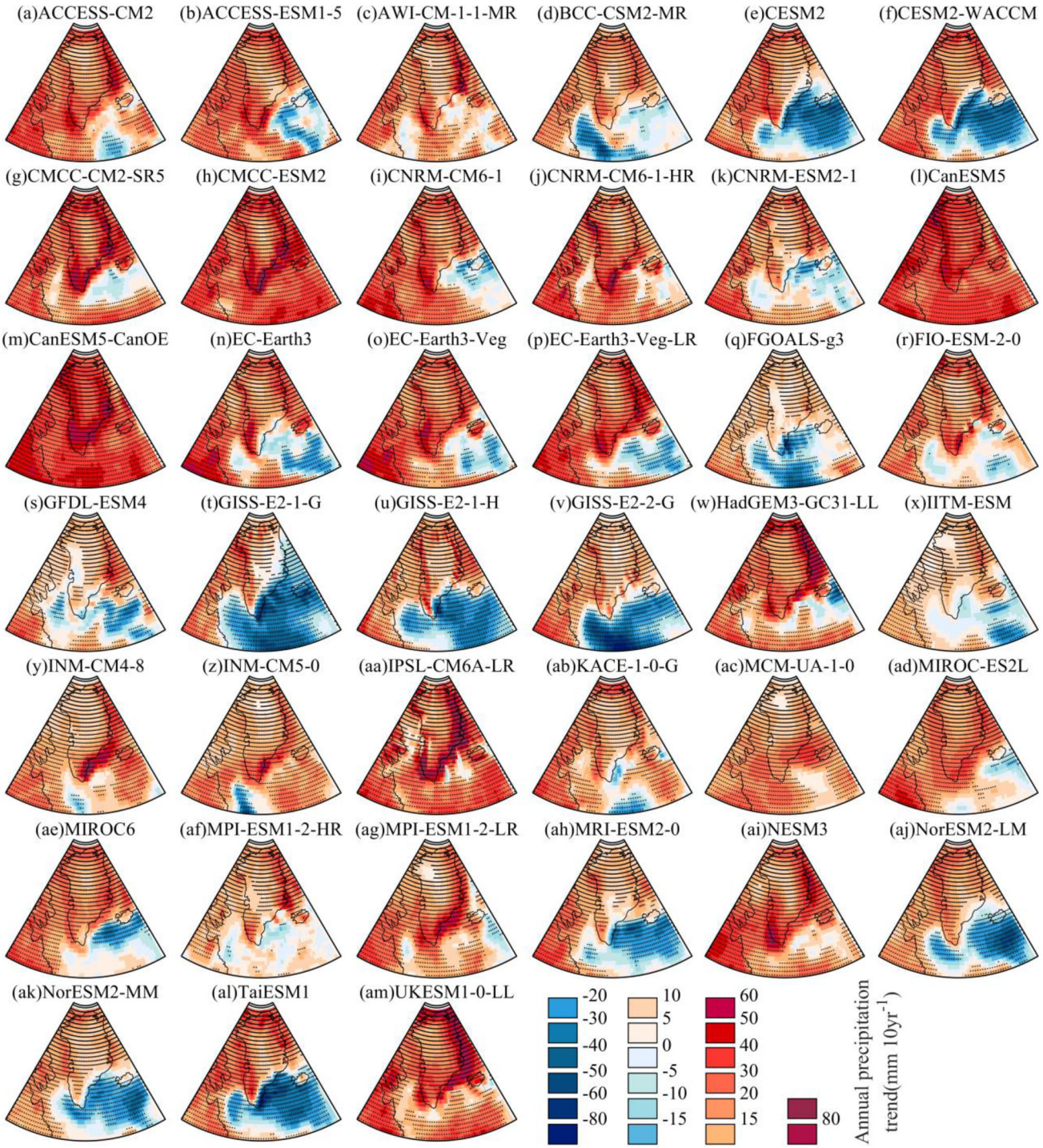

Fig. 1 | Precipitation trends during 2015–2100 with all CMIP6 models under SSP5-85. a–am are the individual CMIP6 model. Black dots represent statistically significant (at 95%) trends.

equatorial Northern Hemisphere (lon: 0°–360°, lat: 20–90°N) and annual precipitation over Greenland (lon: −75° to −10°, lat: 52–85°N) for the periods P1 (1951–1980) and P2 (2071–2100). Note that Fig. 4 highlights results from the CMIP6 model CESM2-WACCM under SSP5-8.5 warming scenario as a case study after analyzing a selection of GCMs in "Methods".

Figure 4 presents patterns and time series of the loading vectors for the leading mode (SVD1) of detrended annual precipitation over Greenland and Z500 in the non-equatorial Northern Hemisphere. SVD1 reflects the Northern Annular Mode NAM signature[44] with the related atmospheric pattern in Northern Hemisphere circulation, and the time series of SVD1 for precipitation and Z500 correlate well with the NAM ($R = 0.74$ for periods P1 and $R = 0.88$ for periods P2, Fig. 4e, f). This confirms a tight coupling between the annual precipitation over Greenland and Z500 in the Northern Hemisphere. The leading mode (SVD1) explains 45% and 48% of the squared covariance fraction (SCF) for periods P1 and P2, respectively, which means that a clear co-variability exists between the northern hemispheric Z500 and annual Greenland precipitation fields on interannual time scales.

The second mode (SVD2) explains 26% and 20% of the SCF for periods P1 and P2, respectively (Fig. 5). While SVD1 represents the NAM, the atmospheric circulation anomalies associated with SVD2 are more regional

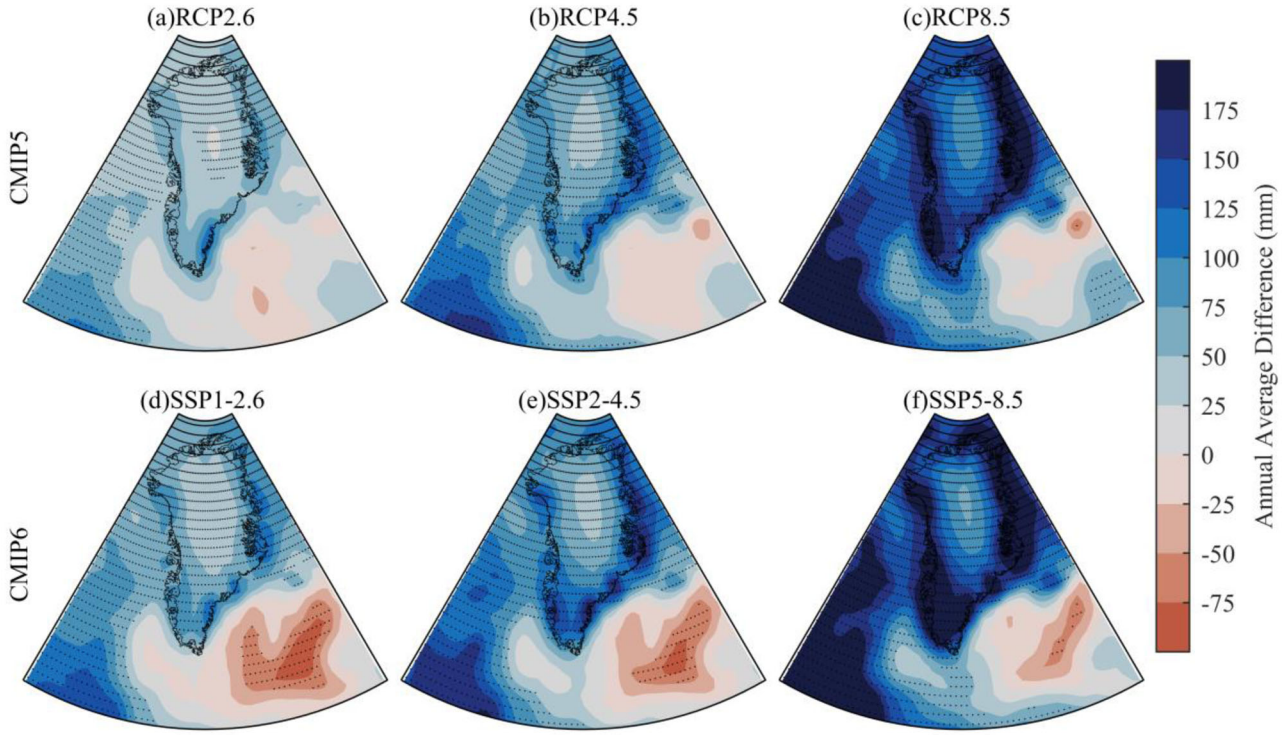

Fig. 2 | Spatial difference in annual precipitation over Greenland between the periods 2071–2100 and 1951–1980. The CMIP5 (with **a** RCP2.6, **b** RCP4.5 and **c** RCP8.5) and CMIP6 (with **d** SSP1-2.6, **e** SSP2-4.5 and **f** SSP5-8.5) model ensemble mean under three warming scenarios, the black dots represent statistically significant (at 95%) trends.

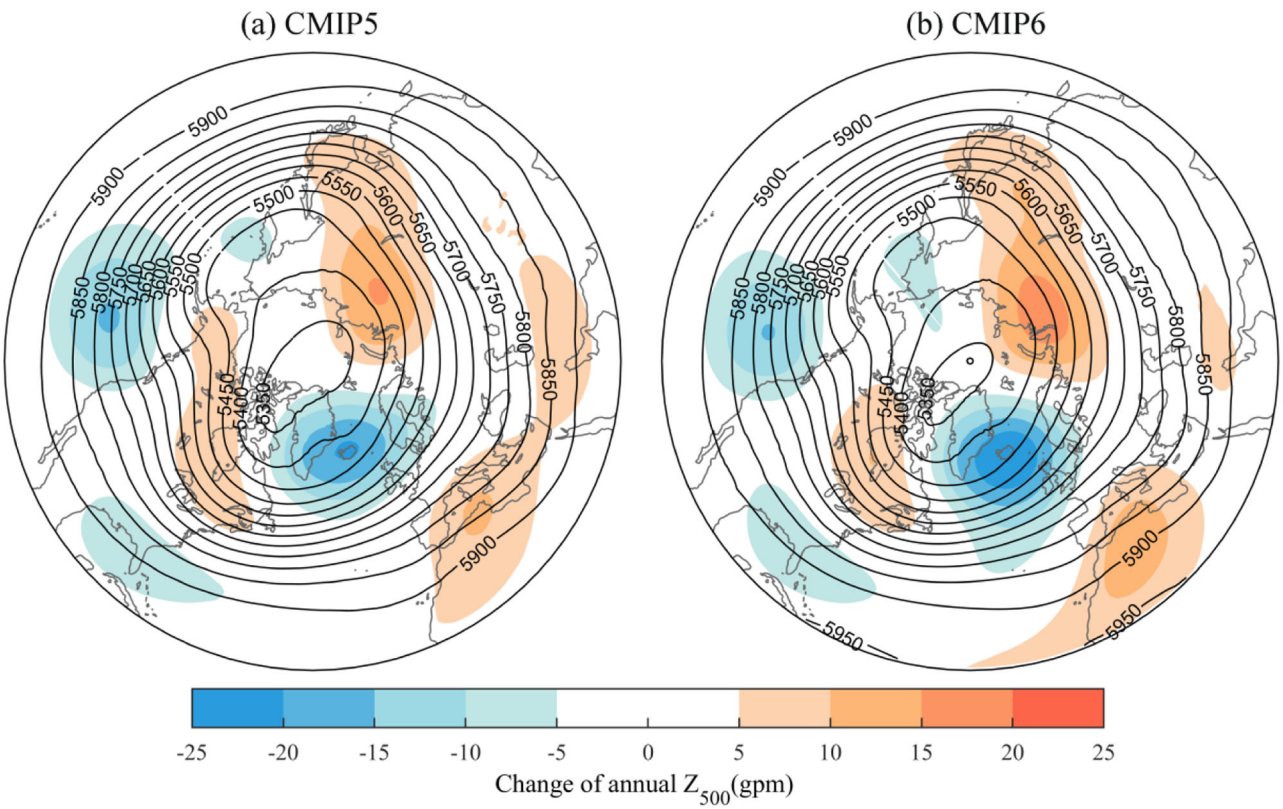

Fig. 3 | Change in 500 hPa geopotential height (Z500) between 2071–2100 and 1951–1980. The CMIP5 (**a**) and CMIP6 (**b**) multi-model ensemble mean under the SSP5-8.5 scenario; solid lines are the projected annual 500 hPa geopotential height for 2071–2100.

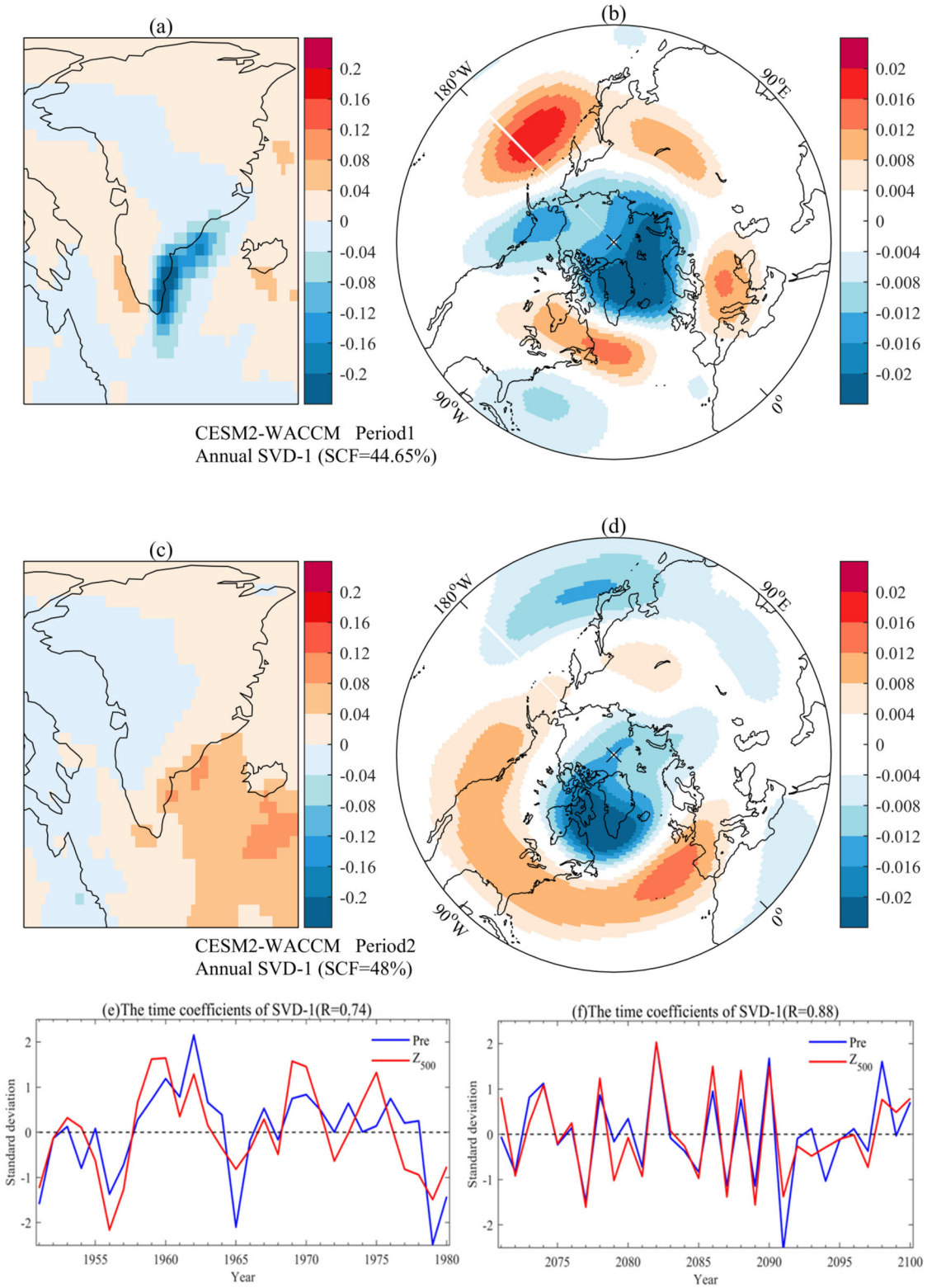

Fig. 4 | Spatial patterns of the leading singular value decomposition mode (SVD1) of the detrended Greenland annual precipitation and Northern Hemisphere Z500. The Greenland annual precipitation with **a** period 1951–1980 and **c** 2071–2100 while the Northern Hemisphere Z500 with **b** period 1951–1980 and **d** 2071–2100 under SSP5-8.5 warming scenario from the CESM2-WACCM model. Time series of the precipitation in Greenland (SVD1) and Northern Hemisphere Z500 **e** period 1951–1980 and **f** 2071–2100. Correlation coefficient *R* passed the significance test.

and similar to the NAO. SVD2 suggests that atmospheric circulation anomalies in period P2 lead to a negative precipitation anomaly in southeast Greenland (Fig. 5c). We conclude that the NAO change shown in SVD2 in period P2 is responsible for the dipole pattern in future precipitation change, with a decrease in southeast and an increase in north/west Greenland.

The SVD2 mode pattern for the two periods shows that this atmospheric circulation anomaly (the eastward and northward shift of the circulation anomalies from period P1 to P2, Fig. 5b, d) leads to an obvious negative signal of precipitation in southeast Greenland during the second period P2 (Fig. 5c). Our hypothesis is that this atmospheric circulation

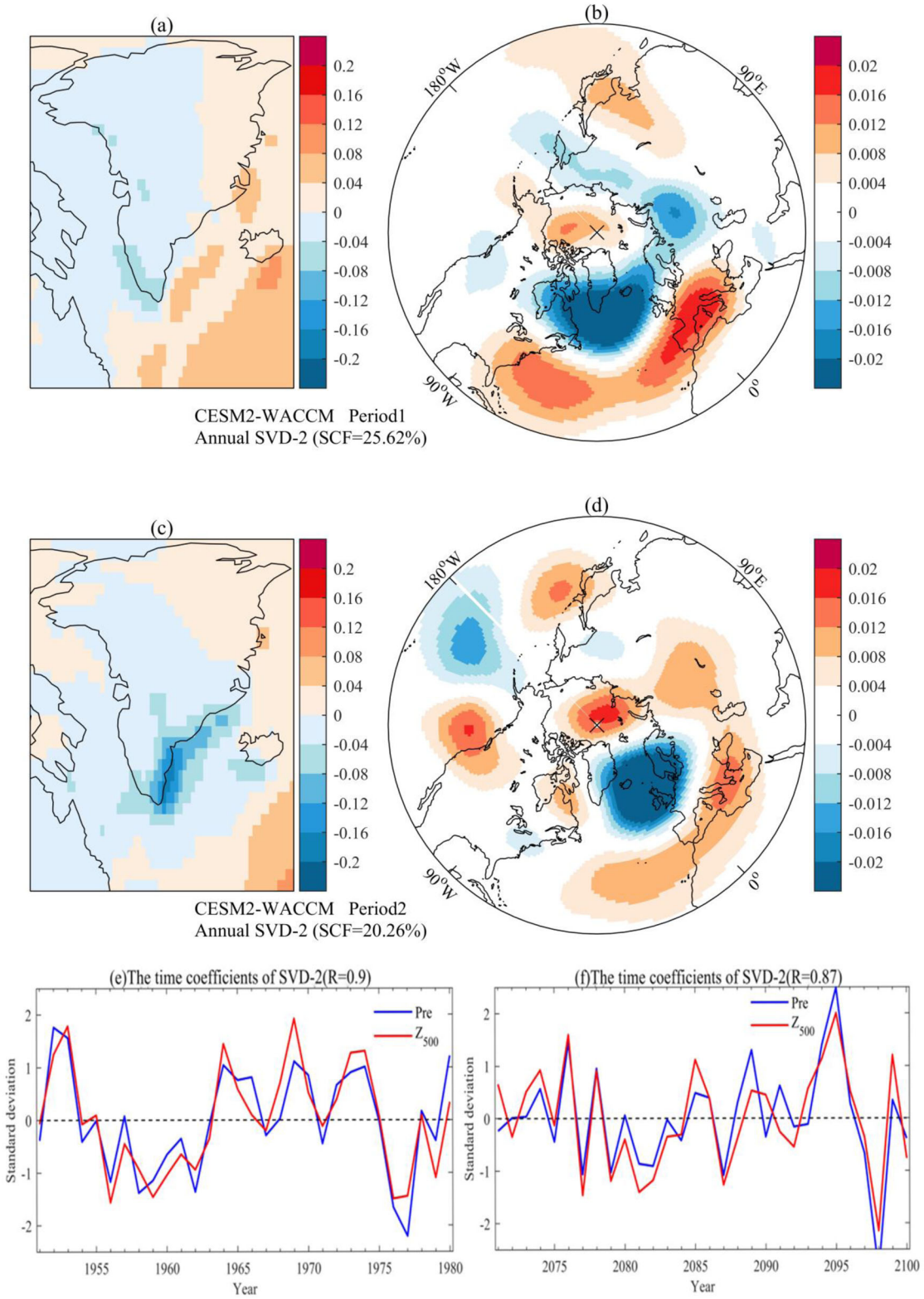

Fig. 5 | Spatial patterns of SVD2 of the detrended Greenland annual precipitation and Northern Hemisphere Z500. The Greenland annual precipitation with **a** period 1951–1980 and **c** 2071–2100 while the Northern Hemisphere Z500 with **b** period 1951–1980 and **d** 2071–2100 under SSP5-8.5 warming scenario from CESM2-WACCM model. Time series of the precipitation in Greenland (SVD2) and Northern Hemisphere Z500 **e** period 1951–1980 and **f** 2071–2100. Correlation coefficient *R* passed the significance test.

anomaly caused the precipitation decrease in southeast Greenland, which suggests a tight coupling between the precipitation in southeast Greenland and atmospheric circulation anomalies over the North Atlantic. SVD2 time series for periods P1 and P2 are strongly correlated ($R = 0.90$ for P1 and $R = 0.87$ for P2, Fig. 5e, f). The tight coupling between atmospheric circulation anomalies over the North Atlantic and precipitation in southeast Greenland implies that the shift in NAO may be a crucial factor influencing the projection of precipitation change in southeast Greenland in the future.

The results presented in Figs. 4 and 5 were derived from an individual model, CESM2-WACCM. To ensure that the results presented are robust, SVD modes of three additional models in CMIP6 (EC-earth3, UKESM1-0-LL, and HadGEM3-GC31-LL) are presented in the Supplementary Material (Figs. S3 and S4). These models consistently show that the SVD2 mode of atmospheric circulation change is responsible for reduced precipitation over southeast Greenland during the second period (2071–2100, Fig. S4).

Circulation anomalies

To identify the mechanisms linking changes in circulation pattern with Greenland precipitation, a more detailed analysis of atmospheric circulation anomalies was performed. Regional precipitation in north and northeast Greenland is influenced by changes in sea ice cover[45], in the southeast by the strength of the IL[46], and in southwest Greenland by cyclogenesis in the Labrador Sea[47]. Previous studies have shown that the IL is a better predictor of southeast Greenland precipitation than climate indices such as the NAO, AH or AMO from regression analysis during 1958-2012[34]. To identify the drivers of the circulation anomaly, we examine the IL and AH pressure systems, i.e., the two centers of action that define the NAO[30].

Figure 6a, b shows the location (latitude and longitude) of the IL and AH using the ensemble mean of the 39 CMIP6 models under the SSP5-8.5 scenario, with a 10-year sliding average. The indices are defined as an area-weighted pressure departure from a threshold, i.e., positive values of the indices indicate that the mean COA location is further to the east and south, and negative values indicate that the COA is further to the west and north. We use standardized simulations for the period 2015–2100 based on the no-mitigation scenario SSP5-8.5. We find a robust northward and eastward shift of both pressure systems under SSP5-8.5. A previous study showed that IL and AH evolution in a global warming projection with the ECHAM4/OPYC3 coupled general circulation model, are both intensified and shifted northeastward by 10° to 20° in latitude and 30° to 40° in longitude in the period 2000–2099[38], which are supportive with the results of this work. The ensemble mean SLP for 1951–1980 (P1) and then 2071–2100 (P2) also indicate an expansion of the IL region, particularly toward the northeast (Fig. 6c, d).

Southeasterly winds from the IL transport moist air towards southeast Greenland and surrounding regions when the IL is located far to the west. In contrast, southeast Greenland experiences drier conditions, when the IL is located farther to the east[47,48]. Storms move farther west and deposit more precipitation on the southeastern coast of Greenland when the low is farther west, and vice versa when the low is farther east[30,34]. Previous studies have shown that a northward shift in the storm track has a drying effect on the southeastern coast of Greenland, with an increase of precipitation over the southwestern coast and the eastern region. This is confirmed by the previous studies that a northward shift in the storm track in the 20th century[49], and studies also predict a northward shift during the 21st century[32,33].

Our results support a northward and eastward shift of the IL under the warming scenario SSP5-8.5 during 2015–2100, which leads to a drying signal over southeast Greenland and surrounding regions. These results are confirmed by the SVD2 patterns of detrended annual precipitation over Greenland and Z500 in the non-equatorial northern Hemisphere from selected CMIP6 models, which all showed decreasing precipitation signals in southeast Greenland during P2 (2071–2100) due to atmospheric circulation changes (Fig. S4).

Discussion

Projecting future precipitation changes over Greenland remains challenging, with large regional differences among climate models[34,50]. Climate models are much less consistent in predicting changes in precipitation than in temperature. Since precipitation is controlled by both temperature (thermodynamic) and circulation (dynamic), the implication is that these inconsistencies mainly arise from differences in the model ability to accurately represent atmospheric circulation patterns[49,51]. For Greenland, a future precipitation increase is considered likely due to thermodynamic changes, e.g., enhanced evaporation when sea ice cover declines, in turn increasing moisture availability to enhance precipitation[24,43]. Previous study found a greater sensitivity of precipitation change to warming in CMIP6 compared to CMIP5 models, with a faster sea ice decline, and larger moisture flux increase to the Arctic in CMIP6[43]. These factors cause an increase in precipitation over eastern and northern Greenland by nearly 60% compared to 1961–1999[24].

Other studies focus on the weakened Atlantic Meridional Overturning Circulation (AMOC) and potentially decreasing SST[52,53]. An emergent constraint between AMOC strength and projected decline suggests a possible AMOC decline between 34% and 45% by 2100[52]. Then a weakened AMOC will reduce evaporation from the ocean and atmospheric eddy moisture transport[54], further impacting the precipitation. Models agree in simulating a drying signal over the subtropical eastern North Atlantic due to AMOC[53]. These precipitation changes are dominated by dynamic changes in atmospheric circulation rather than the thermodynamic changes related to the increase in specific humidity due to global warming[53].

We examined future Greenland precipitation changes in CMIP5 and CMIP6 models, and the linkage to atmospheric circulation anomalies in the Northern Hemisphere. The CMIP6 models were evaluated with precipitation and atmospheric circulation performance to conduct a case study, and results show that CMIP6 have a large inter-model spread. Overall, CESM2-WACCM, UKESM1-0-LL, HadGEM3-GC31-LL, and EC-earth3 simulated precipitation and circulation fields are consistent with the ERA5 climate reanalysis. Our study confirms the large influence of atmospheric circulation anomalies on precipitation changes over Greenland. In the last three decades of the 21st century (2071–2100), the Z500 change from CMIP5 and CMIP6 models is characterized by a widespread increase across the Arctic compared to the baseline period 1951–1980. This is combined with a negative anomaly centered over Iceland and surrounding regions. In northern Greenland, we find a significant positive trend in precipitation in all warming scenarios. In contrast, for the southeastern coast of Greenland, where precipitation is affected by the IL[29,34], the positive trend is insignificant.

The effect of the eastward and northward shift of the IL under SSP5-8.5 is significant, which leads to a drying signal of precipitation over the wider North Atlantic Ocean that extends to the southeastern Greenland margin. Our results corroborate that shifts in the IL location have a strong influence on precipitation production over southeastern Greenland[50,55].

Further work will focus on the moisture transport and sources to verify the spatio-temporal pattern of Greenland precipitation changes[28,56,57]. These findings are beneficial to further understand and improve projections of Greenland precipitation and their impact on future GrIS surface mass balance.

Methods

Datasets

In this study, we used 39 global climate models (GCM) from CMIP6 and 26 models from CMIP5 for which monthly mean precipitation and 500 hPa geopotential heights (Z500) were compared (Table S1 in Supplementary Material). The selection criteria for GCMs are: (1) the availability of the same ensemble members (r1i1p1 for CMIP5 and r1i1p1f1 for CMIP6) to ensure a meaningful comparison; (2) the availability of monthly outputs from both CMIP5 and CMIP6 models of the precipitation (snowfall and rainfall), mean sea level pressure (SLP) and Z500; (3) the availability of the strongest emissions scenario (RCP8.5 and SSP5-8.5).

Compared to the RCPs (the Representative Concentration Pathway) in CMIP5, the SSPs (the Shared Socioeconomic Pathways) consider additional anthropogenic forcing (e.g., land cover/land use) and socioeconomic developments such as population growth and health investments[58]. To investigate the response of precipitation change to circulation anomalies, we use Z500 and mean SLP from RCP8.5 (CMIP5) and SSP5-8.5 (CMIP6), i.e., high-end emission/warming scenarios that increase radiative forcing by 8.5 W m^{-2} in 2100[31,59]. For a more comprehensive analysis of the precipitation change patterns, we also used a low, medium, and high-emission scenario (RCP2.6, SSP1-2.6, RCP4.5, SSP2-4.5, RCP8.5, and SSP5-8.5).

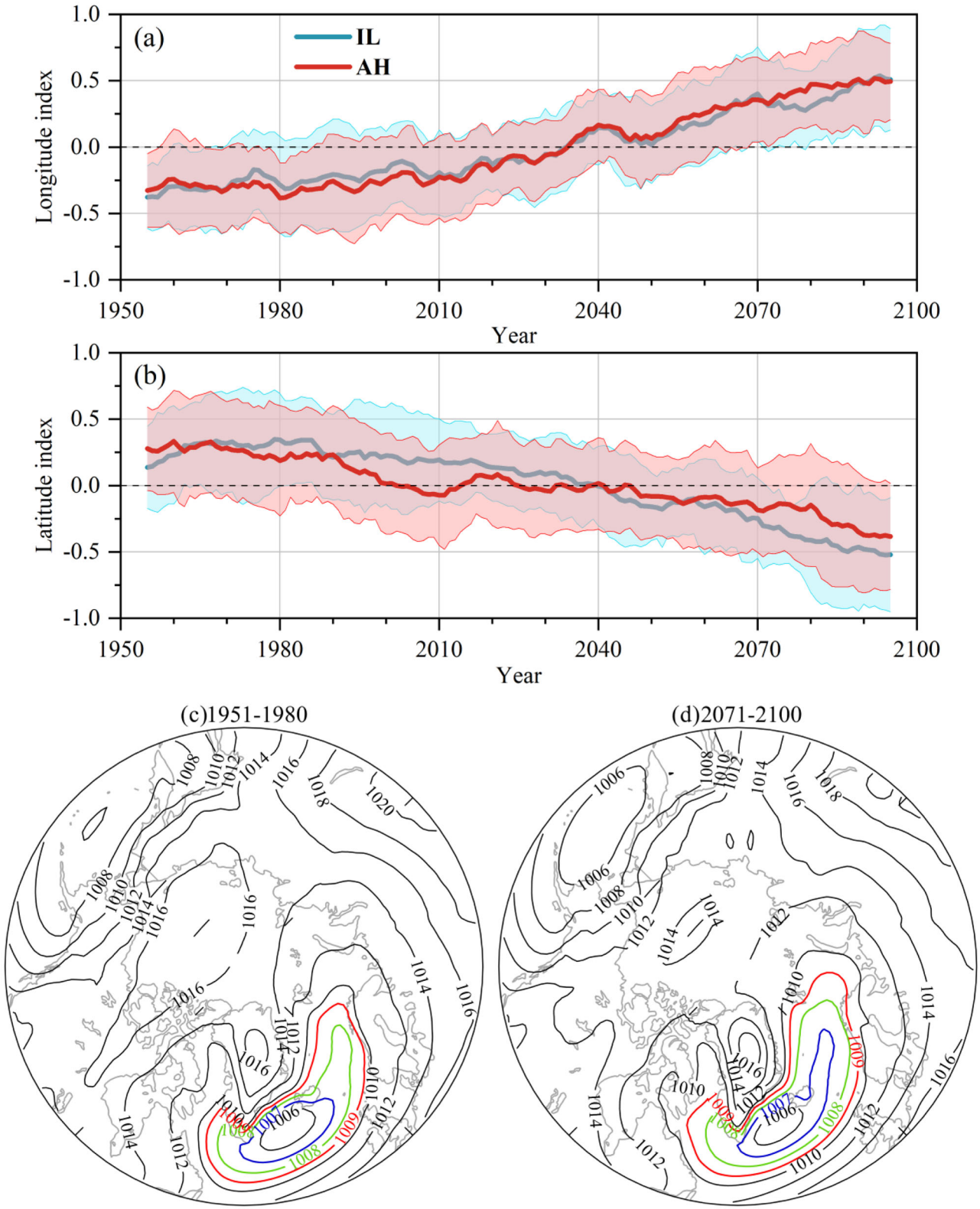

Fig. 6 | The Icelandic low standardized indexes and CMIP6 models ensemble mean SLP (hPa). The longitude (**a**) and latitude (**b**) using the ensemble mean of 39 CMIP6 models under SSP5-85 (the positive longitude means a shift towards the east, and negative latitude a shift towards the north). A 10-year sliding average is applied; the shaded regions represent model uncertainty. CMIP6 models ensemble mean SLP (hPa) under SSP5-85 for 1951–1980 (**c**) and 2071–2100 (**d**) where 1007, 1008 and 1009 hpa contours are displayed in blue, green and red, respectively, in the two maps.

Selection of GCMs/ESMs

Since individual model projections of atmospheric circulation-related fields (including precipitation) show a wide range of possible outcomes (CMIP5 models evaluation)[51], we used multi-model and multi-scenario ensemble means to project future regional precipitation and climate change (Table S1 in Supplementary Material). For a case study analyzing the connections between future Greenland precipitation change and circulation anomaly patterns, individual models were also examined.

Compared to previous CMIPs, the fully coupled Earth System Models (ESM) endorsed by CMIP6 contain more realistic and complete physical processes, as well as a finer spatial resolution[41]. The study has quantitatively evaluated the fidelity with which the NAM is represented in ESM outputs from the CMIP6 archive[42]. They found that ESMs show consistently high skill at capturing NAM spatial and temporal characteristics as observed in the ERA-Interim climate reanalysis. Because of the high co-variation between indices of NAM and NAO[60], they assume that variations of the NAO are well represented by NAM. CESM2-WACCM, EC-earth3, and UKESM1-0-LL were selected as these models are known to reproduce the NAM well[42].

Moreover, Supplementary Fig. S5 shows the performance of the 39 models of CMIP6 in simulating annual mean 500 hPa geopotential heights. Using ERA5 as a reference, we evaluate the historical climatic period 1961–2014 in 39 CMIP6 models. When compared to ERA5 (i.e., CMIP6 minus ERA5), it appears that CESM2-WACCM, HadGEM3-GC31-LL, EC-earth3 and UKESM1-0-LL under the SSP5-8.5 scenario are good candidates to drive atmospheric circulation changes projections, with model discrepancies mostly lower than 2 SD relative to ERA5. Similarly, we evaluate the ability of CMIP6 GCMs to represent precipitation, see the first part of Results section. Previous studies have shown that CMIP6 ESMs consistently have high skill in capturing NAM or NAO[42]. Based on these conclusions and the modeled atmospheric circulation and precipitation evaluation (Figs. S1 and S5), we selected the model CESM2- WACCM for the case study that explores the coupled connections between Greenland precipitation change and the circulation anomaly pattern. The results of the other three models are presented in the Supplementary Material[61].

The period 1951–1980 (P1) was selected as the historic period, i.e., before the start of significant changes in the Greenland climate in the 1990s[62], and the period 2071–2100 at the end of the 21st century was selected as the future period (P2).

Atmospheric circulation anomaly

We used singular value decomposition (SVD), which can efficiently capture the coupled variability between two fields[61,63,64]. Here SVD is used to investigate the dominant coupled patterns between annual precipitation change in Greenland and atmospheric circulation anomalies over the Northern Hemisphere.

The NAO index does not capture the geographically extensive nature of the high- and low-pressure systems and their movements[65]. For instance, the influence of the IL and AH on the climate of the North Atlantic region are quite specific deriving from fluctuations in both their characteristic shapes and positions[65]. As precipitation in southeast Greenland is dominated by the IL[46], we track the location (latitude, longitude) of the IL and the AH[34,37,66]. The pressure index of the IL is defined as an area-weighted pressure departure from a threshold value over its domain (i, j). The location indices give pressure-weighted mean latitudinal and longitudinal positions of the IL. Note that the domains of the AH and IL overlap; the threshold that separates them is 1014 hPa, which means that if the monthly averaged pressure in a grid box is greater than 1014 hPa, it is assigned to the AH, and for a lower value to the IL. The area domains covered by the indices are: the IL (40°N–75°N, 90°W–20°E) and the AH (20°N–50°N, 70°W–10°E). We calculated the indices for the years 1951–2100 with 39 individual models of CMIP6 under the SSP5-8.5 emissions scenario, and then the 10-year sliding average ensemble mean location indices were obtained.

Data availability

All model outputs from CMIP5 and CMIP6 are available from https://esgf-node.llnl.gov/projects/esgf-llnl/.

Code availability

All results and the script of the whole process are available through an email request to the authors.

Received: 12 December 2023; Accepted: 2 January 2025;
Published online: 10 January 2025

References

1. Serreze, M. C. & Barry, R. G. Processes and impacts of Arctic amplification: a research synthesis. *Glob. Planet. Change* **77**, 85–96 (2011).
2. Hofer, S. et al. Greater Greenland Ice Sheet contribution to global sea level rise in CMIP6. *Nat. Commun.* **11**, 6289 (2020).
3. Van den Broeke, M. et al. Greenland ice sheet surface mass loss: recent developments in observation and modeling. *Curr. Clim. Change Rep.* **3**, 345–356 (2017). 2017.
4. Lenaerts, J. T. M., Medley, B., van den Broeke, M. R. & Wouters, B. Observing and modeling ice sheet surface mass balance. *Rev. Geophys.* **57**, 376–420 (2019).
5. Mouginot, J. et al. Forty-six years of Greenland Ice Sheet mass balance from 1972 to 2018. *Proc. Natl. Acad. Sci. USA* **116**, 9239–9244 (2019).
6. Slater, T., Hogg, A. E. & Mottram, R. Ice-sheet losses track high-end sea-level rise projections. *Nat. Clim. Change* **10**, 879–881 (2020).
7. Noël, B., van Kampenhout, L., Lenaerts, J. T. M., van de Berg, W. J. & Van Den Broeke, M. R. A 21st century warming threshold for sustained Greenland ice sheet mass loss. *Geophys. Res. Lett.* **48**, e2020GL090471 (2021).
8. Fettweis, X. et al. Estimating the Greenland ice sheet surface mass balance contribution to future sea level rise using the regional atmospheric climate model MAR. *Cryosphere* **7**, 469–489 (2013).
9. Rignot, E., Velicogna, I., van den Broeke, M. R., Monaghan, A. & Lenaerts, J. Acceleration of the contribution of the Greenland and Antarctic ice sheets to sea level rise. *Geophys. Res. Lett.* **38**, L05503 (2011).
10. Box, J. E. et al. Greenland ice sheet surface mass balance variability (1988–2004) from calibrated polar MM5 output. *J. Clim.* **19**, 2783–2800 (2006).
11. Van den Broeke, M. et al. Partitioning recent Greenland mass loss. *Science* **326**, 984–986 (2009).
12. Hines, K. M. & Bromwich, D. H. Development and testing of Polar Weather Research and Forecasting (WRF) model. Part I: Greenland ice sheet meteorology [J]. *Monthly Weather Rev.* **136**, 1971–1989 (2008).
13. Franco, B., Fettweis, X., Erpicum, M. & Nicolay, S. Present and future climates of the Greenland ice sheet according to the IPCC AR4 models. *Clim. Dyn.* **36**, 1897–1918 (2011).
14. Fettweis, X., Galle, H., Lefebre, L. & van Ypersele, J. P. Greenland surface mass balance simulated by a regional climate model and comparison with satellite derived data in 1990–1991. *Clim. Dyn.* **24**, 623–640 (2005).
15. Bintanja, R. The impact of Arctic warming on increased rainfall. *Sci. Rep.* **8**, 6–11 (2018).
16. Bintanja, R. & Selten, F. M. Future increases in Arctic precipitation linked to local evaporation and sea-ice retreat. *Nature* **509**, 479–482 (2014).
17. Van den Broeke, M. R. et al. On the recent contribution of the Greenland ice sheet to sea level change. *Cryosphere* **10**, 1933–1946 (2016).
18. Montgomery, L., Koenig, L., Lenaerts, J. T. & Munneke, P. K. Accumulation rates (2009–2017) in Southeast Greenland derived from airborne snow radar and comparison with regional climate models. *Ann. Glaciol.* **61**, 225–233 (2020).
19. Fettweis, X. et al. GrSMBMIP: intercomparison of the modelled 1980–2012 surface mass balance over the Greenland Ice Sheet. *Cryosphere* **14**, 3935–3958 (2020).
20. Csatho, B. M. et al. Laser altimetry reveals complex pattern of Greenland Ice Sheet dynamics. *Proc. Natl. Acad. Sci. USA* **111**, 18478–18483 (2014).

21. Lewis, G. et al. Recent precipitation decrease across the Western Greenland ice sheet percolation zone. *Cryosphere* **13**, 2797–2815 (2019).
22. Pattyn, F. et al. The Greenland and Antarctic ice sheets under 1.5 C global warming. *Nat. Clim. Change* **8**, 1053–1061 (2018).
23. Doyle, S. et al. Amplified melt and flow of the Greenland ice sheet driven by late-summer cyclonic rainfall. *Nat. Geosci.* **8**, 647–653 (2015).
24. Schuenemann, K. C. & Cassano, J. J. Changes in synoptic weather patterns and Greenland precipitation in the 20th and 21st centuries: 2. Analysis of 21st century atmospheric changes using self-organizing maps. *J. Geophys. Res.* **115**, D05108 (2010).
25. Bengtsson, L., Hodges, K. I., Koumoutsaris, S., Zahn, M. & Keenlyside, N. The changing atmospheric water cycle in Polar Regions in a warmer climate. *Tellus A: Dyn. Meteorol. Oceanogr.* **63**, 907–920 (2011).
26. Kattsov, V. M. et al. Simulation and projection of Arctic freshwater budget components by the IPCC AR4 global climate models. *J. Hydrometeorol.* **8**, 571–589 (2007).
27. Collins, M., Knutti, R., Arblaster, J., Dufresne, J.-L., Fichefet, T., Friedlingstein, P., Gao, X., Gutowski, W.J., Johns, T.,Krinner, G., Shongwe, M., Tebaldi, C., Weaver, A.J., & Wehner, M. (2013). Chapter 12 - Long-term climate change:Projections, commitments and irreversibility. In: Climate Change 2013: The Physical Science Basis. IPCC Working Group I Contribution to AR5. Eds. IPCC, Cambridge: Cambridge University Press..
28. Mattingly, K. S. et al. Strong summer atmospheric rivers trigger Greenland ice sheet melt through spatially varying surface energy balance and cloud regimes. *J. Clim.* **33**, 6809–6832 (2020).
29. Auger, J. D., Birkel, S. D., Maasch, K. A., Mayewski, P. A. & Schuenemann, K. C. Examination of precipitation variability in southern Greenland,. *J. Geophys. Res. Atmos.* **122**, 6202–6216 (2017).
30. Serreze, M. C., Carse, F., Barry, R. G. & Rogers, J. C. Icelandic low cyclone activity: Climatological features, linkages with the NAO, and relationships with recent changes in the Northern Hemisphere circulation. *J. Clim.* **10**, 453–464 (1997).
31. McKenna, C. M. & Maycock, A. C. Sources of uncertainty in multimodel large ensemble projections of the winter North Atlantic Oscillation. *Geophys. Res. Lett.* **48**, e2021GL093258 (2021).
32. Yin, J. H. A consistent poleward shift of the storm tracks in simulations of 21st century climate. *Geophys. Res. Lett.* https://doi.org/10.1029/2005GL023684 (2005).
33. Alley, R. et al. Climate change 2007: The physical science basis. In *Contribution of Working Group I to the Fourth Assessment Report of the Intergovernmental Panel on Climate Change. Summary for Policymakers* (IPCC Secretariat, Geneva, Switzerland, 2007).
34. Berdahl, M. et al. Southeast Greenland winter precipitation strongly linked to the Icelandic low position. *J. Clim.* **31**, 4483–4500 (2018).
35. Bromwich, D. H., Chen, Q. S., Li, Y. & Cullather, R. I. Precipitation over Greenland and its relation to the North Atlantic Oscillation. *J. Geophys. Res.: Atmos.* **104**, 22103–22115 (1999).
36. Appenzeller, C., Schwander, J., Sommer, S. & Stocker, T. F. The North Atlantic Oscillation and its imprint on precipitation and ice accumulation in Greenland. *Geophys. Res. Lett.* **25**, 1939–1942 (1998).
37. Bakalian, F., Hameed, S. & Pickart, R. Influence of the Icelandic Low latitude on the frequency of Greenland tip jet events: Implications for Irminger Sea convection. *J. Geophys. Res.* **112**, C04020 (2007).
38. Hu, Z. Z. & Wu, Z. The intensification and shift of the annual North Atlantic Oscillation in a global warming scenario simulation. *Tellus A: Dyn. Meteorol. Oceanogr.* **56**, 112–124 (2004).
39. Meehl, G. A., Boer, G. J., Covey, C., Latif, M. & Stouffer, R. J. The coupled model intercomparison project (CMIP). *Bull. Am. Meteorol. Soc.* **81**, 313–318 (2000).
40. Taylor, K. E., Stouffer, R. J. & Meehl, G. A. An overview of CMIP5 and the experiment design. *Bull. Am. Meteorol. Soc.* **93**, 485–498 (2012).
41. Eyring, V. et al. Overview of the Coupled Model Intercomparison Project Phase 6 (CMIP6) experimental design and organization. *Geosci. Model Dev.* **9**, 1937–1958 (2016).
42. McCrystall, M. R., Stroeve, J., Serreze, M., Forbes, B. C. & Screen, J. A. New climate models reveal faster and larger increases in Arctic precipitation than previously projected. *Nat. Commun.* **12**, 6765 (2021).
43. Krinner, G. & Julien, N. High-resolution simulations of the surface mass balance of Greenland at the end of this century. *Cryosphere Discuss.* **1**, 351–383 (2007).
44. Coburn, J. & Pryor, S. C. Differential credibility of climate models in CMIP6. *J. Clim.* **34**, 8145–8164 (2021).
45. Zwally, H. J. & Giovinetto, M. B. Balance mass flux and ice velocity across the equilibrium line in drainage systems of Greenland. *J. Geophys. Res.* **106**, 33717–33728 (2001).
46. Huai, B., van den Broeke, M. R., Reijmer, C. H. & Noël, B. A daily 1-km resolution Greenland rainfall climatology (1958–2020) from statistical downscaling of a regional atmospheric climate model. *J. Geophys. Res.: Atmos.* **127**, e2022JD036688 (2022).
47. Hanna, E., McConnell, J., Das, S., Cappelen, J. & Stephens, A. Observed and modeled Greenland ice sheet snow accumulation, 1958–2003, and links with regional climate forcing. *J. Clim.* **19**, 344–358 (2006).
48. Gorter, W., Van Angelen, J. H., Lenaerts, J. T. M. & Van den Broeke, M. R. Present and future near-surface wind climate of Greenland from high resolution regional climate modelling. *Clim. Dyn.* **42**, 1595–1611 (2014).
49. Wang, X. L., Swail, V. R. & Zwiers, F. W. Climatology and changes of extratropical cyclone activity: comparison of ERA-40 with NCEP–NCAR reanalysis for 1958–2001. *J. Clim.* **19**, 3145–3166 (2006).
50. Bromwich, D. H., Cullather, R. I., Chen, Q. S. & Csathó, B. M. Evaluation of recent precipitation studies for Greenland ice sheet. *J. Geophys. Res.: Atmos.* **103**, 26007–26024 (1998).
51. Shepherd, T. G. Atmospheric circulation as a source of uncertainty in climate change projections. *Nat. Geosci.* **7**, 703–708 (2014).
52. Weijer, W., Cheng, W., Garuba, O. A., Hu, A. & Nadiga, B. T. CMIP6 models predict significant 21st century decline of the Atlantic meridional overturning circulation. *Geophys. Res. Lett.* **47**, e2019GL086075 (2020).
53. Bellomo, K., Angeloni, M., Corti, S. & von Hardenberg, J. Future climate change shaped by inter-model differences in Atlantic meridional overturning circulation response. *Nat. Commun.* **12**, 3659 (2021).
54. Hand, R., Keenlyside, N. S., Omrani, N. E., Bader, J. & Greatbatch, R. J. The role of local sea surface temperature pattern changes in shaping climate change in the North Atlantic sector. *Clim. Dyn.* **52**, 417–438 (2019).
55. Chen, Q. S., Bromwich, D. H. & Bai, L. Precipitation over Greenland retrieved by a dynamic method and its relation to cyclonic activity. *J. Clim.* **10**, 839–870 (1997).
56. Bintanja, R. et al. Strong future increases in Arctic precipitation variability linked to poleward moisture transport. *Sci. Adv.* **6**, eaax6869 (2020).
57. Box, J. E. et al. Greenland ice sheet climate disequilibrium and committed sea-level rise. *Nat. Clim. Change* **12**, 808–813 (2022).
58. Aadhar, S. & Mishra, V. On the projected decline in droughts over South Asia in CMIP6 multimodel ensemble. *J. Geophys. Res.: Atmos.* **125**, e2020JD033587 (2020).
59. O'Neill, B. C. et al. The scenario model intercomparison project (ScenarioMIP) for CMIP6. *Geosci. Model Dev.* **9**, 3461–3482 (2016).
60. Wallace, J. M. & Thompson, D. W. Annular modes and climate prediction. *Phys. Today* **55**, 28–33 (2002).

61. Bretherton, C. S., Smith, C. & Wallace, J. M. An intercomparison of methods for finding coupled patterns in climate data. *J. Clim.* **5**, 541–560 (1992).
62. Zhang, Q. et al. Temporal and spatial variability in contemporary Greenland warming (1958–2020). *J. Clim.* **35**, 2755–2767 (2022).
63. Cherry, S. Some comments on singular value decomposition analysis. *J. Clim.* **10**, 1759–1761 (1997).
64. Yang, J., Liu, T., Dou, T. & Xiao, C. Interannual variability of winter precipitation over the Lambert Glacier basin linked to the dipole pattern of sea surface temperature in the southern Indian Ocean. *Front. Earth Sci.* **10**, 920245 (2022).
65. Iqbal, M. J. & Rashid, S. F. A re-interpretation of impact of the Icelandic Low and Azores High on winter precipitation over Iberian Peninsula. *Arab. J. Geosci.* **9**, 1–7 (2016).
66. Hameed, S. & Piontkovski, S. The dominant influence of the Icelandic low on the position of the Gulf Stream northwall. *Geophys. Res. Lett.* **31**, L09303 (2004).

Acknowledgements

The authors acknowledge support from the Netherlands Earth System Science Centre (NESSC) and PROTECT, this project has received funding from the European Union's Horizon 2020 Research and Innovation program. This work was also funded by the Natural Science Foundation of China (42171121), Taishan Scholars Program of Shandong province and the Outstanding Youth Fund project of Shandong province (ZR2023YQ035). B. Noël was funded by the Fonds de la Recherche Scientifique de Belgique (F.R.S.-FNRS).

Author contributions

B.H., M.R.v.d.B., C.H.R., B.N., and M.D. coordinated the study. B.H. drafted the paper, and M.R.v.d.B., C.H.R., B.N., and M.D. edited the paper. W.S. and Y.W. made revisions to the paper. All authors contributed to the analysis, discussion and interpretation of the results.

Competing interests

The authors declare no competing interests.

Additional information

Supplementary information The online version contains supplementary material available at https://doi.org/10.1038/s41612-025-00899-z.

Correspondence and requests for materials should be addressed to Minghu Ding.